Colorimetric and SERS Based Multimode Detection Platform for Cu (II) Ions Using Peptide-Gold Nanoparticles

Panangattukara Prabhakaran Praveen Kumar *

Posted Date: 14 August 2025

doi: 10.20944/preprints202508.1109.v1

Keywords: peptides; gold nanoparticles; copper; colorimetric response; Raman based detection; singlet oxygen; photodynamic therapy

 doi:10.20944/preprints202508.1109.v1

Article

Colorimetric and SERS Based Multimode Detection Platform for Cu (II) Ions Using Peptide-Gold Nanoparticles

Panangattukara Prabhakaran Praveen Kumar [1,2]

[1] KU-KIST Graduate School of Converging Science and Technology, Korea University, 145 Anam-ro, Seongbuk-gu, Seoul 02841, Republic of Korea; pananga1@msu.edu or p4praveen.18@gmail.com

[2] Department of Biomedical Engineering, Institute for Quantitative Health Science and Engineering, Michigan State University, East Lansing, MI 48824, USA

Abstract

Excessive copper ions in the human body can cause variety of diseases such as gastrointestinal disorders, cirrhosis, and Alzheimer's diseases. Techniques like Inductively Coupled Plasma Mass, and Atomic Absorption Spectroscopy are available for copper detection, but the associated cost issue for sample preparation and labor limited their application for on-site detection. Herein we are reporting a versatile method for detecting copper ions using a peptide-functionalized gold nanoparticle sensor in combination with various optical spectroscopic techniques. The peptide (CW) showed a selective sensing ability for Cu (II) with visual colorimetric and optical spectroscopic changes as compared with other metal ions tested. CW showed a visual colorimetric response from colorless to light brown color after interaction with Cu (II). Converting CW to gold nanoparticle appended (CW-AuNPs) nanoplatform allowed a multimode detection platform for Cu (II) which utilizes colorimetric, optical spectrum changes, and surface-enhanced Raman spectroscopy (SERS) to enable highly sensitive sensing of Cu (II), even at extremely low concentrations (76 nM). CW-AuNPs exhibit a controlled aggregation property in the presence of Cu (II), resulting in the creation of hot spots for SERS-based detection. Moreover, the peptide unit attached to the gold nanoparticles serves both as a binding motif for Cu (II) and as a Raman reporter for Cu (II) sensing. Our comprehensive analysis, including solution-state and dry-mapping Raman spectroscopic studies, demonstrates remarkable picomolar sensitivity of the peptide-gold nanoparticle system for Cu (II) detection. Moreover, we prepared a paper test strip from CW-AuNPs and used it as a visual colorimetric platform for sensitive detection of copper ions. The CW-AuNPs-Cu (II) nanoaggregate was used as a photodynamic therapy agent (PDT) for invitro studies with a singlet oxygen quantum yield of 0.21%.

Keywords: peptides; gold nanoparticles; copper; colorimetric response; Raman based detection; singlet oxygen; photodynamic therapy

1. Introduction

Metal ion sensing carries significant implications across diverse fields. While many metal ions contribute to vital biochemical reactions, a few pose hazards and toxicity risks [1,2]. Essential trace elements such as zinc, copper, and manganese are crucial for living organisms, yet their concentrations beyond optimal levels can lead to adverse effects [3]. Among these metals, copper finds wide industrial applications, but its environmental accumulation can result in severe environmental and health concerns [4,5]. Consequently, the development of sensitive and selective detection methods for copper becomes imperative to ensure environmental safety and human well-being. Although standard techniques like atomic absorption spectroscopy [6], inductively coupled plasma-mass spectrometry [7,8], and voltametric techniques [9] offer favorable detection limits for a broad concentration range, they suffer from drawbacks such as costly sample preparation, time-

 doi:10.20944/preprints202508.1109.v1

consuming procedures, and the need for bulky equipment . These techniques are unsuitable for on-site applications, and specialized methods are required for biological sample evaluation. Progress in science has yielded novel detection platforms, including colorimetric [10,11], fluorometric [12,13], magnetic resonance imaging [14,15], and strip-based techniques [16,17]for metal ion detection.

Gold nanoparticles (AuNPs) have gained significant attention as promising materials in biosensing applications due to their unique optical and electronic properties [18,19]. The utilization of colorimetric assays with AuNPs has become an appealing approach for detecting a wide range of analytes. Their strong surface-plasmon resonance peaks (SPR) enable monitoring of minute molecular level changes. The selection of AuNPs is justified by their ability to exhibit size tunable optical properties and undergo surface modifications. Notably, surface functionalization of AuNPs with peptides offers specific recognition and binding sites for target analytes [20,21]. Peptides are highly desirable ligands for biosensing applications due to their exceptional selectivity, stability, and multiple binding sites [22,23]. By combining the plasmonic nature of AuNPs with the metal binding properties of peptides, various metal ion sensors can be fabricated. Peptide capped AuNPs provide tunability for metal ion sensing by facilitating multipoint interactions between peptides and different metal ions. This assay platform offers advantages such as sensitivity, rapid in situ metal ion detection, and visible color changes resulting from NP aggregation. The surface functionalities can be adjusted using a range of peptides to induce such aggregation [24,25].

The alteration of SPR peaks of AuNPs directly determines the associated color change when they bind to metals. This change can be attributed to factors such as variations in particle size, shape, surface chemistry, or interparticle distance during aggregate formation [26]. Consequently, these modifications in the SPR peaks play a pivotal role in significantly enhancing the Raman scattering of molecules near the AuNPs or aggregates through Surface Enhanced Raman Spectroscopy (SERS) [27,28]. SERS-based sensors have proven to meet the essential requirements for metal ion sensing, including high sensitivity, selectivity, and suitability for on-site applications, and for biomedical applications [29–31]. The fundamental principle underlying this technique lies in the observed alterations in the Raman spectrum of the material adsorbed on the SERS active nanomaterial upon binding with the analyte. The distinctive spectral features of the adsorbed material, in combination with the SERS activity, enable the development of sensitive and accurate assays for detecting metal ions [32–34].

In this study, we present a peptide-Au-based nanoparticle system for the selective detection of Cu (II) ions in aqueous media. The dipeptide (**CW**) containing cystine and tryptophan as backbone without AuNPs showed excellent binding property towards Cu (II) ions. After conjugating **CW** with AuNPs, we demonstrated a colorimetric and Raman-based detection assay with high sensitivity and reproducibility for Cu (II) detection. While previous studies have explored the use of various nanoparticles for Cu (II) detection, the application of SERS for sensitive and onsite detection is relatively scarce. Our peptide-Au nanoparticle (**CW-AuNPs**) system provides a versatile platform for Cu (II) ion detection, employing multiple optical spectroscopy techniques and Raman spectroscopy. The nanoparticles were carefully designed to ensure excellent dispersity, indicating no non-specific interactions between the peptide and Au. Upon the addition of Cu (II) ions, we observed selective aggregation of the Au nanoparticles, distinguishing Cu (II) from other metal ions. Our solution-based SERS measurements demonstrated picomolar sensitivity, while dry-state Raman mapping studies showed femtomolar sensitivity.

2. Materials and Methods

2.1. General Techniques

^{1}H, ^{13}C NMR spectra were recorded on a Bruker Avance II 500 MHz NMR spectrometer at 25 °C. Absorption spectra were recorded on a Shimadzu UV-2600 UV-visible spectrophotometer in 3 mL quartz cuvettes with a path length of 1 cm. Emission spectra were recorded on Hitachi F7000 instrument with slit width of 2 nm. Circular dichroism (CD) spectra were recorded on JASCO J-

 doi:10.20944/preprints202508.1109.v1

815spectropolarimeter. Fluorescence lifetimes were measured by the time-correlated single-photon counting (TCSPC) technique on a Deltaflex modular fluorescence lifetime system from HORIBA Scientific using a nano-LED pulse diode light source. The instrument response function (IRF) of the setup was 200 ps and measured using 1% ludox (colloidal silica) solution. For dynamic light scattering analysis, a Malvern Zetasizer 2000 DLS spectrometer equipped with a 633 nm CW laser was employed. Transmission electron microscopic images were obtained using Hitachi (Tokyo, Japan), H-7100 series TEM instrument. Raman spectral data were acquired using an inverted Raman microscope (NOST, South Korea) equipped with a 60× objective lens (0.6 numerical aperture, Olympus, Tokyo, Japan). A 633 nm laser (CNI Laser, China) was employed to excite the sample solution. The resulting scattered Raman signals were collected through a 100 μm confocal motorized pinhole and directed to a spectrometer (FEX-MD, NOST, South Korea) fitted with a 1200 g mm^{-1} grating. The final signal detection was carried out using a charge-modified device camera (Andor DV401A-BVF, Belfast, Northern Ireland).

2.2. Materials

Metal perchlorates, HEPES buffer, $HAuCl_4$, $NaBH_4$, 3-(4,5-dimethylthiazolyl-2)-25-diphenyl tetrazolium bromide (MTT), calcein AM, propidium iodide, singlet Oxygen Sensor green (SOSG), Methylene blue were purchased from Sigma-Aldrich.

2.3. Synthesis of CW

CW was prepared from previous literature reports [31,35]. **CW** is characterised using ^{1}HNMR, ^{13}CNMR, and by mass spectrometry. ^{1}HNMR: (500 MHz, D_2O) ppm δ: 3.06 (dd, J = 15.0, 7.5 Hz, 2H), 3.17 (m, 4H), 3.24 (m, 2H), 3.63 (s, 6H), 4.47 (m, 2H), 4.71 (br s, 2H), 7.09 (s, 2H), 7.18 (s, 4H), 7.45 (br d, 2H), 7.52 (br d, 2H).; 13CNMR (125 MHz, D_2O): 26.48, 37.83, 51.49, 52.96, 53.94, 108.68, 111.94, 118.21, 119.35, 121.98, 124.48, 126.75, 136.10, 167.66, 173.19. HRMS calcd. for $C_{30}H_{37}N_6O_6S_2$, m/z = 641.2211, obtained m/z = 641.2241

2.4. Metal Ion Binding Studies Using UV-Visible and Emission Spectroscopy

Solutions of **CW** were prepared in HEPES buffer (pH = 7.4) at a concentration of 10μM. Similarly, metal perchlorate solutions (60 μM) were also prepared in HEPES buffer. These metal ions were gradually added to the solutions of **CW** and for titration. UV-Vis absorption spectra were recorded throughout the process using a Shimadzu UV-2400 double-beam spectrophotometer. Titration was carried out until no further spectral changes were observed, indicating saturation. A similar experiment was performed for emission spectroscopy studies, were the samples excited at 290 nm and spectrum recorded using Hitachi F7000 instrument with slit width of 2 nm.

2.5. Determination of Stoichiometry of Complex

An equimolar Solutions of **CW**, and Metal perchlorate were prepared in HEPES buffer (10 μM). The mole fraction of **CW** was systematically adjusted from 0.1 to 1. After applying the necessary correction factors, the corresponding changes in absorbance were recorded and plotted as a function of receptor mole fraction.

2.6. Estimation of Binding Constant via Benesi-Hildebrand Approach

The binding affinity between compound 4 and dopamine was evaluated using UV-Visible spectroscopy, applying the Benesi-Hildebrand equation. This method enables the calculation of the association constant (K) by analyzing changes in absorbance. The relationship used is:

$$1/ A_0\text{-}A = 1/(A_0\text{-}A_\infty)K[G]+ 1/(A_0\text{-}A_\infty) \text{ ----------(1)}$$

In this equation, A and A_0 are the absorbance values of **CW** in the presence and absence of Cu(II), respectively, while A_∞ denotes the absorbance at saturation (infinite dilution with Cu(II)).

 doi:10.20944/preprints202508.1109.v1

2.7. Calculation of Limit of Detection (LOD)

The limit of detection (LOD) for dopamine using compound 4 was determined based on the standard method:

$$LOD = K*Sb/k. \text{ ---------- } (2)$$

Here, K is a constant (typically 3), S_b represents the standard deviation of the blank (ligand-only) solution, and k is the slope derived from the calibration curve. This calculation provides a measure of the sensor's sensitivity to low concentrations of Cu(II).

2.8. Preparation of CW-AuNPs

An aqueous solution of **CW** (3mL, 0.5 mM) was subjected to reduction using $NaBH_4$ (0.2 mL, 10 mM) in the presence of $HAuCl_4$ (1.8 mL, 0.5 mM). This reaction resulted in the formation of CW-AuNPs which was confirmed form the visual response of the reaction from colorless to light pink color.

2.9. SERS-Based Detection

For the surface-enhanced Raman scattering (SERS)-based detection of Cu(II), **CW**-AuNPs (50 µg) was incubated with varying concentrations of Cu(II) ranging from 10^{-6} M to 10^{-15} M. These samples were then drop-cast onto glass slides using a silicone isolator. Raman spectra were recorded using a 633 nm laser (6.8 mW, 10 s exposure time) and a 60× objective lens. Following drying, the solid residues containing **CW**-AuNPs and bound Cu(II) were subjected to Raman mapping. A region approximately 1.5–2.0 mm in diameter on each glass slide was scanned at 25 × 25 pixels resolution, with 10 seconds of exposure per pixel. Raman mapping images were generated based on the intensity at 1414 cm^{-1}.

2.10. Investigation of Singlet Oxygen Generation

Stock solutions of photosensitisers and the reference dye, methylene blue (MB), Singlet Oxygen Sensor Green (SOSG) were prepared in water. In a typical experiment, 1.8 mL of the aqueous photosensitizer solution was transferred to a cuvette, followed by the addition of 0.2 mL of SOSG solution. After recording the initial fluorescence, the sample was exposed to light from a Xenon lamp equipped with a 475 nm cut-off filter. The increse in emission for SOSG 520 nm was tracked over time to evaluate singlet oxygen generation.

2.11. Cell Culture

The breast cancer cell line f was maintained in Dulbecco's Modified Eagle's Medium, supplemented with 10% fetal bovine serum and 1% antibiotic–antimycotic solution. The cultures were incubated at 37 °C in a humidified atmosphere with 5% CO_2 and subcultured twice a week.

2.12. Live and Dead Cell Assay

MDA-MB-231 cells were cultured in 24-well plates at a density of 20,000 cells per well and incubated overnight at 37 °C with 5% CO_2. The next day, the cells were exposed to CW-AuNPs-Cu(II) at a concentration of 50 µg/mL and incubated for 1 hour. Afterward, the wells were rinsed with PBS, followed by irradiation using an 808 nm laser at 2 W/cm^2 for 1 minute. The cells were then returned to the incubator and maintained overnight under the same conditions. On the third day, post-treatment, the cells were again washed and stained with 1 µM calcein AM and 2 µM propidium iodide and fluorescence imaging was performed.

 doi:10.20944/preprints202508.1109.v1

3. Results

3.1. Characterisation and Photophysics for CW

CW was synthesized following previous literature reports and were characterized by ^{1}H, ^{13}C-NMR and mass spectrometry technique (**Scheme S**1, **Figures S1-S3**). **CW** was fully soluble in water and in HEPES buffer due to the presence of free amino groups in the backbone. **CW** exhibited an absorption peak at 290 nm, corresponding to the tryptophan unit (**Figure S3A**). Additionally, excitation at 290 nm resulted in a monomer emission band at 330 nm corresponds to tryptophan fluorescence (**Figure S3B**). CD spectral studies indicated a random coil structure for **CW**, with a positive band at 220 nm and a negative band at 197 nm (**Figure S3C**). The design strategy for **CW** relies on the metal ion binding property of the disulfide bond, free amine group and the ability of indole unit to form cation-pi interactions. Furthermore, the fluorescence properties of tryptophan make it suitable as a signaling unit after the binding event. The disulfide bond can be easily cleaved using reducing agents, enabling the thiolate peptide to be anchored to AuNPs for sensing applications by taking advantage of the surface plasmon properties of AuNPs for sensing applications.

3.2. Metal Ion Detection Using Spectroscopic Techniques

Following the characterization of **CW**, we proceeded to examine the optical spectroscopic response of **CW** when exposed to various metal ions in HEPES buffer (10 mM, pH 7.5). Among the various tested metal ions (Na(I),K(I), Cs(I), Mg(II), Ba(II), Ag(I), Cd(II), Zn(II), Pb(II), Mn(II), Cu(II), Hg(II), Fe(II), Co(II), Fe(III)); Cu (II) was found to induce changes in the absorption spectra as shown in **Figure S5A**. The addition of Cu (II) resulted in a red shift in the absorption spectrum, accompanied by the emergence of new absorption bands at 460 nm (**Figure 1A**). These higher wavelength absorption bands indicated an interaction between Cu(II) and **CW**, resulting a metal-induced aggregation of **CW**. This aggregation resulted in a slight color change from colorless to light brown for the Cu(II)-**CW** aggregates (**Figure 1A** inset). To confirm the peptide aggregation, scanning electron microscopy studies were conducted, revealing changes in the morphological features of **CW** (**Figure 1B-C**). **CW** showed vesicle like morphology with an average diameter of vesicle from 700-800 nm (**Figure 1B**). It is widely acknowledged that peptides containing tryptophan can form vesicles due to the pi-pi interaction of indole rings [31,36]. However, the interaction of Cu(II) disrupted this pi stacking due to the strong binding of Cu (II) with the indole rings resulted in aggregation of **CW** (**Figure 1C**) [23,31]. Consequently, the peptide aggregation caused discernible chiroptical changes in the CD spectrum of CW, characterized by an inversion of CD signal by the addition of Cu (II) (**Figure 1D**). This chiroptical changes is due to the structural rearrangement and conformational changes in **CW** because of Cu(II) binding. There are studies which showed that copper binding to amyloid-β peptides can induce β-sheet formation with a chiroptical changes in the spectroscopic signals, in a similar way **CW** showed a chiral optical inversion after Cu(II) binding [37,38].

Emission spectroscopy studies provided further insights into Cu (II) sensing. Among the various tested metal ions introduction Cu (II) resulted in a reduction of fluorescence intensity at 330 nm, after the Cu (II) interaction (**Figure 2A and Figure S5B**). Notably, the addition of Hg (II) also led to fluorescence quenching, suggesting their ability to bind with **CW**. To confirm this binding properties in detail we performed time-resolved spectroscopy experiments for **CW** with Cu(II) and Hg(II). The studies showed the observed quenching after Cu (II) binding is due to a static type since there was no change in the lifetime of the monomer emission peak at 330 nm after the addition of Cu (II), indicating a complex formation between **CW** and Cu (II) (**Figure 2B**, **Table S1**). Whereas addition of Hg(II) induced a change in fluorescence lifetime for **CW**, indicate there is a dynamic quenching which can be attributed to the random collison between **CW** and Hg (II) [23,31]. Thus, the observed change in fluorescence with Hg(II) is due to the paramagnetic properties of Hg(II) rather than complex formation with **CW (Table S1)**. The response of **CW** to Cu (II) exhibited linearity within the concentration range of 0 to 6.0×10^{-7} M, with a detection limit of 0.3 μM (**Figure S6A**). The association

 doi:10.20944/preprints202508.1109.v1

constant for **CW** with Cu (II) was calculated using the BindFit model for supramolecular interactions [39,40]. The supramolecular BindFit model showed an accurate fitting data for a 1:1 stoichiometry with an association constant of 4.91×10^{4} M^{-1} which was further supported by the Benesi-Hildebrand association constant values (4.86×10^{4} M^{-1}) (**Figure S6B-C**). The stoichiometry of **CW**-Cu(II) complex was confirmed further by Jobs plot analysis, and it showed a 1:1 stoichiometry with an inflation points at 0.5 molefraction value (**Figure S6D**).

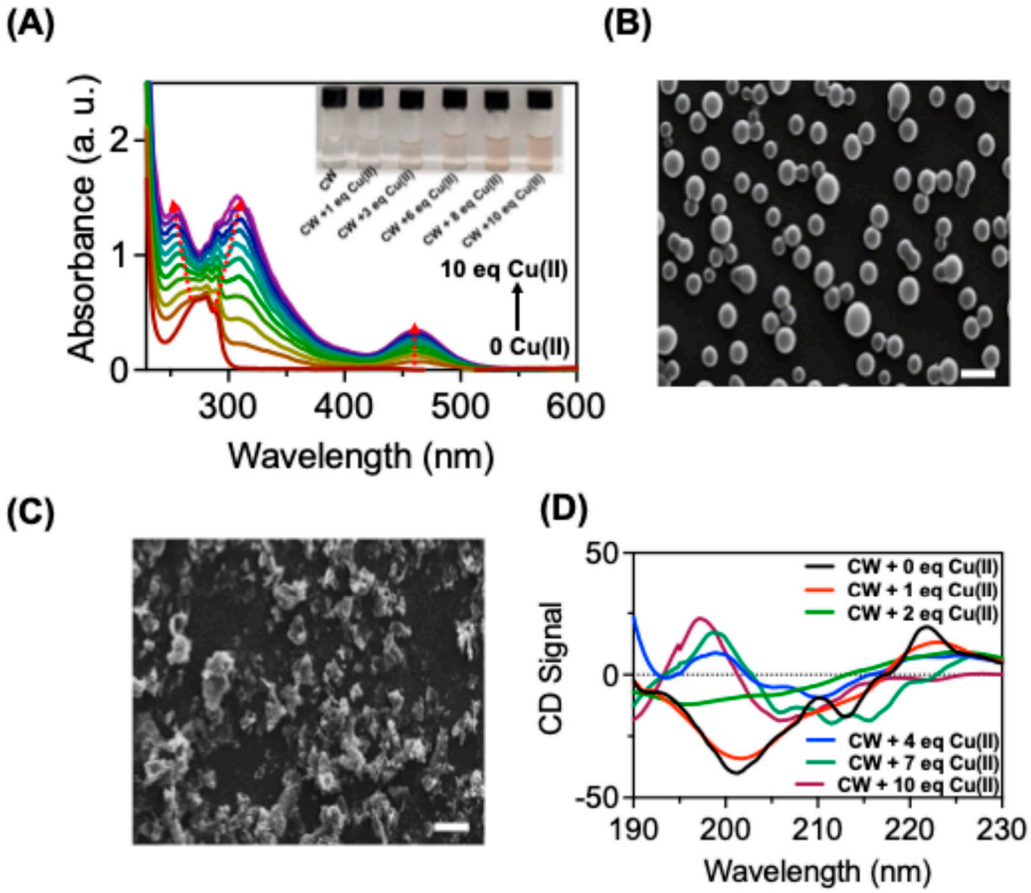

Figure 1. Binding studies for **CW** with Cu(II). (A) Changes in the absorption spectra for **CW** ($10\text{x}10^{-6}$M) alone and with various amount of $Cu(ClO_4)_2{\cdot}6H_2O$ in HEPES buffer (pH =7.4). Scanning electron microscopy images for **CW** without (B) and (C) with $Cu(ClO_4)_2{\cdot}6H_2O$ [60 µM]. Scale bar 1 µm. (D) Circular dichroism spectra for **CW** ($60\text{x}10^{-6}$ M) alone and with addition of various amounts of $Cu(ClO_4)_2{\cdot}6H_2O$.

The binding mode of Cu (II) with **CW** was investigated through ^{1}HNMR studies in D_20 (**Figure 2C**). **CW** showed distinctive NMR peaks for the -S-CH_2 proton at 3.26, and 2.98 ppm. Addition of 0.5 equivalent of Cu (II) resulted in down field shift of the –S-CH_2- protons by 0.3 ppm indicating a strong interaction between Cu (II) and –S atom in Cystine moiety. Further addition of Cu (II) resulted in an increased multiplicity of the –S-CH_2- protons. The aromatic protons in the tryptophan moiety showed considered up field because of the Cu (II) binding after addition of 2 equivalents of Cu(II). It's well known that tryptophan can induce cation-pi interactions, and this interaction induced an up-field shift of the aromatic protons due to the developed ring current in tryptophan moiety after Cu(II) binding.

 doi:10.20944/preprints202508.1109.v1

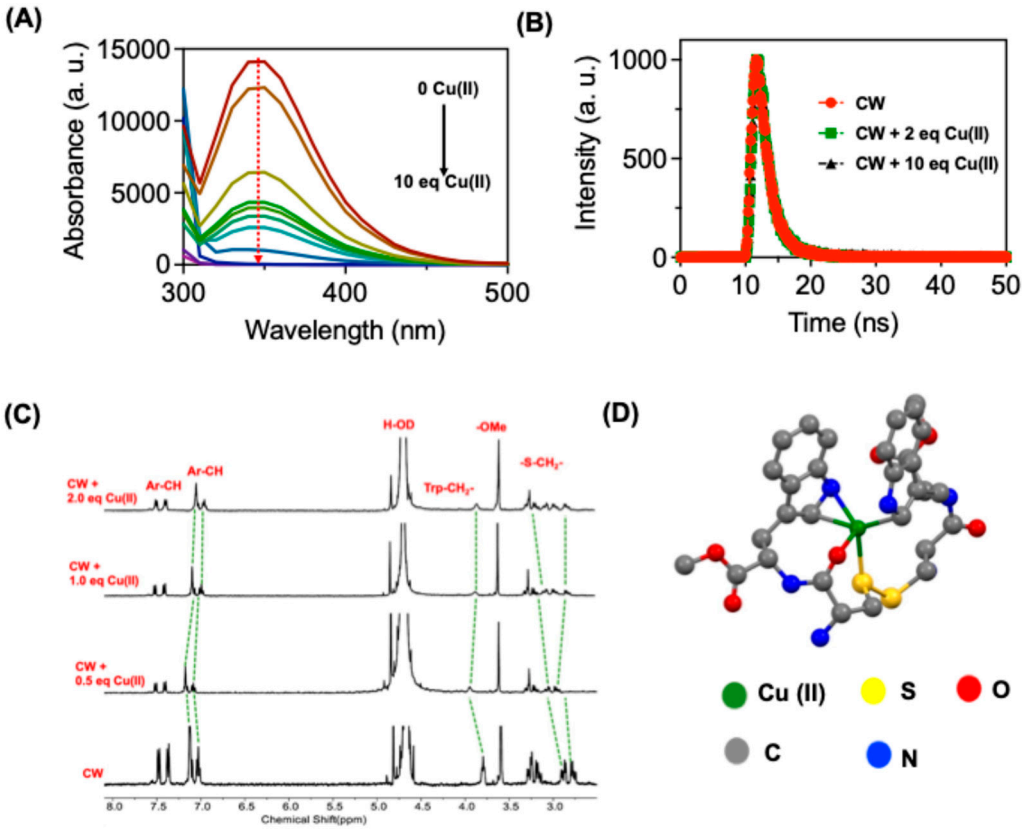

Figure 2. Binding studies for **CW** with Cu(II). (A) Changes in the emission spectra for CW ($10x10^{-6}$M) alone and with various amount of $Cu(ClO_4)_2 \cdot 6H_2O$ in HEPES buffer (pH =7.4). (B) Time resolved spectra for **CW** with Cu(II). (C) Partial ^{1}H-NMR spectra for **CW**, and **CW** with various amounts of Cu(II). The NMR experiments were performed in D_2O. The green dotted lines indicate the changes in NMR peak positions for **CW** and after the addition of Cu(II). (D) Optimized structure for the **CW** with Cu(II).

To validate the complex formation, we have performed density functional theory (DFT) calculations for **CW**-Cu (II) complex (**Figure 2D**). The DFT studies were performed using Gaussian 09 implying B3LYP functional. C, N, O, S and H atoms were6-31G(d) basis set while Cu was treated with Lanl2dz basis set. DFT studies showed that Cu(II) (green color) possess a distorted square pyramidal structure, where Cu(II) ions were coordinated with one of the sulphur atoms from cysteine (yellow color), indole carbon atoms (grey color), indole nitrogen atom (blue color) and with carbonyl oxygen atoms (red color). It should be noted that Cu(II) form a three membered ring structure with indole ring from tryptophan, indicating a delocalized pi electron cloud for the stabilization. Thus, the observed complex multiplicity in NMR spectra for the S-CH_2 proton and the upfield shift for aromatic indole protons can be explained as follows from the DFT studies. The NMR resonance peaks for -S-CH_2- in the complex is due to the presence of both uncomplexed and complexed -S-CH_2- with Cu (II) ions with **CW**. Only one of the -S- atom is involved in coordination with Cu(II). The up-field shift observed for the indole aromatic ring proton is due to the ring current developed in the indole moiety after Cu (II) binding.

3.3. Surface Plasmon Resonance Based Detection

In recent years, there has been a significant advancement in the field of sensing applications with the development of nanoparticles. These nanoparticles have gained attention due to their surface plasmon resonance peaks (SPR), which exhibit a strong and easily detectable color change with analytes. This unique characteristic allows for a straightforward and practical nanoparticle-based detection technique. Among various nanoparticles, gold nanoparticles (AuNPs) showed potential

 doi:10.20944/preprints202508.1109.v1

sensing applications since it offers advantages such as affordability, a wide range of color tunability and easy surface modifications for sensing applications. The colorimetric response observed in nanoparticle-based detection techniques is attributed to two main factors. Firstly, the color change occurs because of the direct interaction between AuNPs and the analyte being detected [18]. Alternatively, the analyte may interact with surface-capped functionalities on the AuNPs, leading to the aggregation of nanoparticles [41]. To enhance stability and introduce desired functionalities, ligands are often added to the surface of AuNPs such as amines, thiols, hydroxyl, etc. This intrigued us to investigate effect of disulfide bond (-S-S-) in **CW** which can be easily reduced to thiol -SH bond and can attach to AuNPs [42]. This modification not only imparts stability but also enhances the detection sensitivity for metal ions through the strong coupling effect of SPR bands from Au and the absorption features of **CW**. Consequently, the colorimetric response of AuNPs can be effectively utilized for the detection of Cu (II).

3.3.1. Synthesize of CW-AuNPs and Photophysics

An aqueous solution of **CW** (3mL, 0.5 mM) was subjected to reduction using $NaBH_4$ (0.2 mL, 10 mM) in the presence of $HAuCl_4$ (1.8 mL, 0.5 mM). This reaction resulted in the formation of **CW**-AuNPs which was confirmed form the visual response of the reaction from colorless to light pink color (**Figure 3A** inset). The UV-Visible spectrum exhibited a SPR band at 550 nm indicating the presence of AuNPs (**Figure 3A**). To determine the size of the AuNPs, transmission electron microscopy (TEM) and dynamic light scattering (DLS) experiments were performed. **CW**-AuNPs showed a hydrodynamic diameter of 105.63 nm with a polydispersity index of 0.082, indicating a highly disperse and stable particles (**Figure 3B**). TEM analysis revealed an average size of 45.1 nm for **CW**-AuNPs (**Figure 3B inset**). Fluorescence spectra were recorded for **CW**-AuNPs, and excitation of CW-AuNPs at 290 nm, showed an emission spectra with maximum at 405 nm (**Figure 3C**). Compared with the emission spectra of **CW**, the **CW**-ANPs showed emission peak at 405 nm indicate a strong aromatic π-π stacking interactions on the metal surface resulting in an excimer emission peak rather than monomer emission compared to **CW** [43].

To investigate the capping of **CW** onto the surface of the AuNPs, Fourier Transform Infrared Spectroscopy (FTIR) and Raman spectroscopy were utilized. FTIR studies showed the characteristic peptide peaks on the surface of AuNPs (**Figure S7**). IR peaks at 1639 and 1522 cm^{-1} corresponds to the amide I and amide II bending vibrations from the **CW** functional group. A similar IR peaks were observed in the **CW**-AuNPs with slight shift in the peak positions such as 1630 for amide I stretching and 1528 for amide II bending indicated successive capping of **CW** on AuNPs. Raman spectroscopy was used to provide additional evidence for the capping of **CW** on the AuNPs (**Figure 3D**). The characteristic Raman peak at 497 cm^{-1}, corresponding to the disulfide bond, was absent in the **CW**-AuNPs spectrum, indicating the formation of a -S-Au bond. The peaks observed at 1010 indole ring breathing vibration, 1270 and 1326 corresponds to the -CH rocking vibrations in the Raman spectrum were attributed to the Raman peaks of tryptophan which further confirmed the successful capping of **CW** on the surface of AuNPs [44]. The slight shifts in peak position of **CW**-AuNPs compared with **CW** indicates the interaction of **CW** with AuNPs.

3.3.2. Metal Ion Sensing for CW-AuNPs

Subsequently, our research focused on exploring the potential of **CW**-AuNPs as a means of detecting metals in HEPES buffer solution (10 mM, pH 7.5). Among the various metal ions tested, the introduction of Cu(II) to **CW**-AuNPs triggered a noticeable color change from pink to bluish, due to the plasmonic properties of Au (**Figure 4A**). Addition of Cu(II) resulted in dramatical changes in the absorption spectrum for **CW**-AuNPs, with the formation of absorption bands at higher wavelengths (**Figure 4B**). The formation of higher wavelength absorption band indicated the aggregation of AuNPs as it was visible from the observed color change from pink to blue. There were no changes in color and absorption spectrum features of **CW**-AuNPs by the addition of other metal ions, indicating the selectivity of **CW**-AuNPs for Cu (II) detection because of the peptide binding moieties on the

 doi:10.20944/preprints202508.1109.v1

surface of AuNPs. **CW**-AuNPs showed a linear relation with the absorbance at 550 nm various concentrations of Cu(II) from with a limit of detection 0.076 μM for Cu(II) (**Figure 4C**). There is a visual colorimetric response was observed depending on the concentration of Cu(II) added in to **CW**-AuNPs due to the strong coupling of SPR properties of **CW**-AuNPs with metal ions (**Figure 4C** inset).

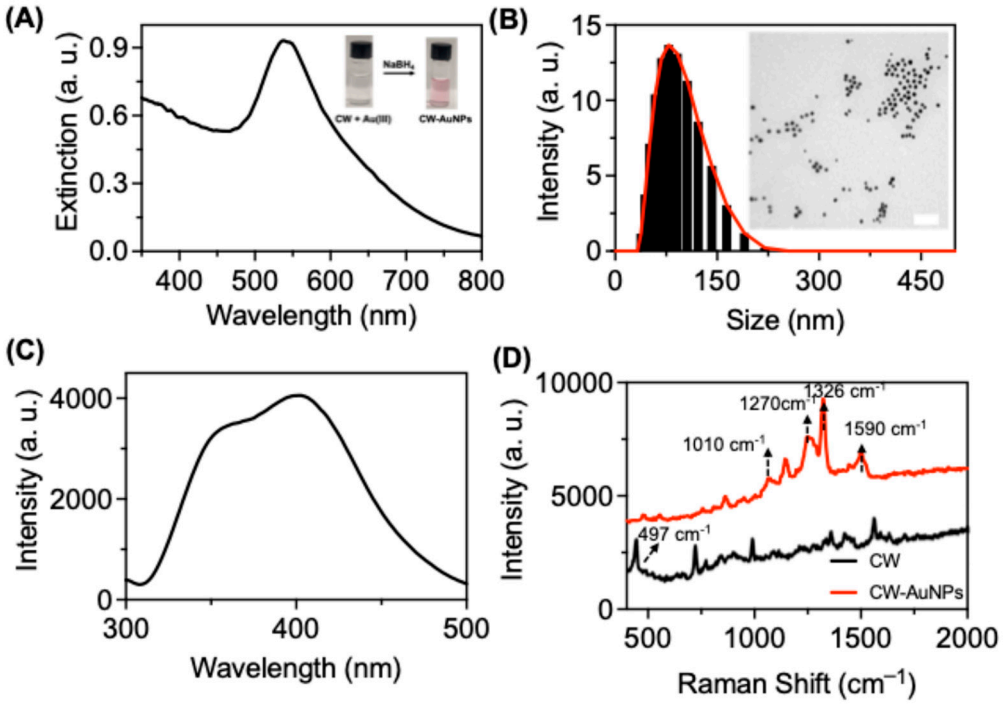

Figure 3. Characterization for **CW**-AuNPs. (A) Extinction spectra for **CW**-AuNPs (100 μg/mL) in HEPES buffer. (B) Dynamic light scattering measurement for **CW**-AuNPs. The inset showing transmission electron microscopic image for **CW**-AuNPs. Scale bar 100 nm. (C) Emission spectra for **CW**-AuNPs (100 μg/mL) in HEPES buffer. λ_{exc} = 290 nm. (D) Raman spectrum for **CW**, and **CW**-AuNPs. Data were collected using a laser source of excitation at 633 nm laser (6.8 mW); Exposure time: 10 s.

As another detection mode next we have utilized the fluorescence from **CW**-AuNPs as a signal reader for the copper detection. The excimer peak at 410 nm corresponding to the tryptophan excimer quenched after Cu(II) addition indicated a strong interaction between **CW**-AuNPs and Cu(II) (**Figure 4D**). By incorporating **C**W into AuNPs, we achieved an enhanced sensitivity for the copper detection as compared with **CW** alone. The selectivity of **CW**-AuNPs with various metal ions were further validated from the colorimetric, UV and emission-based studies, but **CW**-AuNPs showed a selectivity towards Cu(II) (**Figures S8A**-B). Through competitive binding experiments with other metal ions, we demonstrated that **CW**-AuNPs can selectively detect Cu(II), even in the presence of other metal ions (**FigureS8A-B**). TEM studies showed that addition of Cu(II) induced aggregation of NPs and which supports the formation of higher wavelength absorption bands and the observed colorimetric response with Cu(II) (**Figure 4E**).

 doi:10.20944/preprints202508.1109.v1

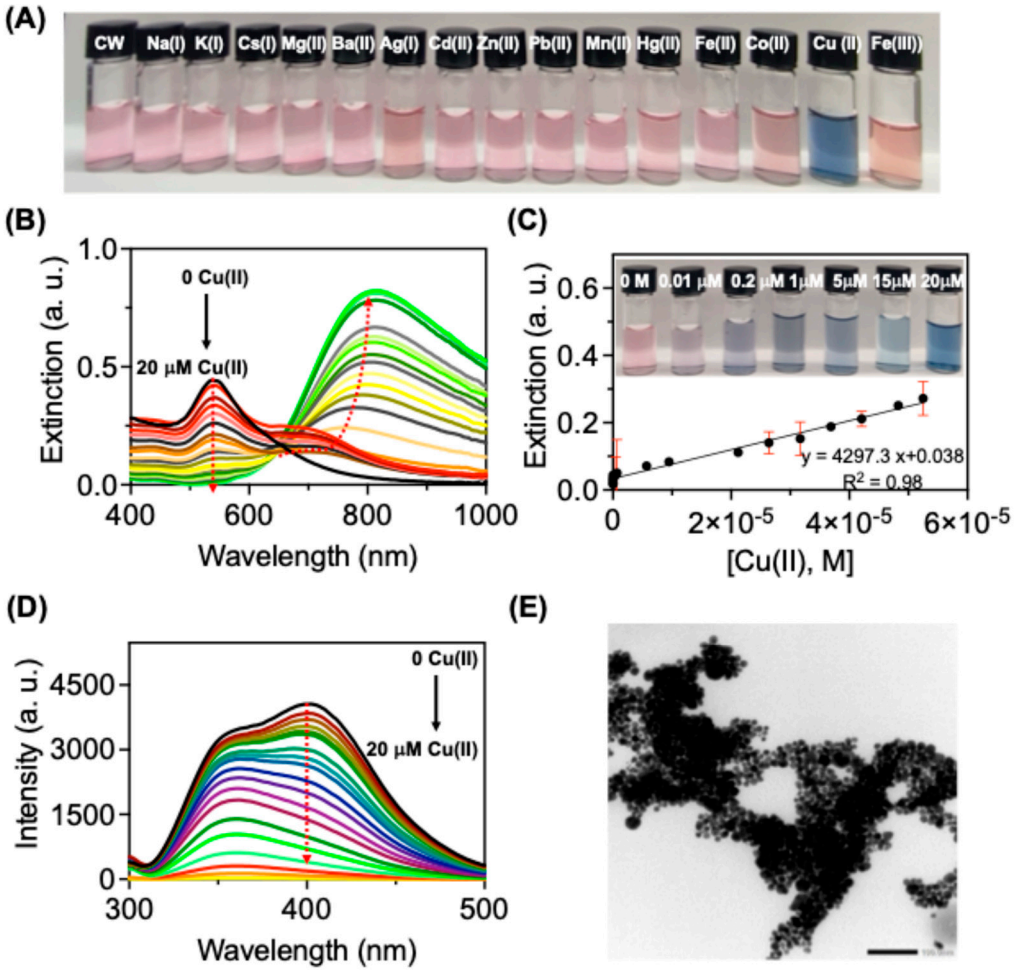

Figure 4. Metal sensing properties of **CW**-AuNPs. (A) Visual colorimetric response for **CW**-AuNPs with various metal ions. [**CW**-AuNPs (100 mg/mL); Metal ions 20 μM]. (B) Changes in the extinction spectra for **CW**-AuNPs with Cu(II), where [**CW**-AuNPs (100 mg/mL); Cu(II) 20 μM]. (C) A quantitative measurement for the detection of Cu(II) using CW-AuNPs. Inset showing the visual colorimetric response of CW-AuNPs with various amount of Cu(II) added. (D) Changes in the emission spectra for **CW**-AuNPs with Cu(II), where [**CW**-AuNPs (100 μg/mL); Cu(II) 20 μM].λ_{exc} = 290 nm. (E) TEM micrographs for CW-AuNPs with Cu(II). Scale bar 100 nm.

3.3.4. Paper Strip Based Colorimetric Response for Cu(II)

Paper strip-based sensing platforms offer a low-cost, portable, and user-friendly approach for detecting metal ions, making them ideal for on-site and point-of-care applications. These strips require minimal sample volume and enable rapid visual readouts through color changes, eliminating the need for complex instrumentation. Their biodegradable nature ensures environmental sustainability, while the surface can be easily functionalized for selective and sensitive detection. Additionally, they demonstrate good shelf-life and can be engineered for multiplexed sensing, further enhancing their practicality in diverse analytical settings.

For practical application we have developed test strips coated with **CW**-AuNPs. For this a Whatman filter paper was immersed in a solution of **CW** (3 mL, 0.5mM) and incubated for an hour at room temperature. Afterwards a solution of $HAuCl_4$ (1.8 mL, 0.5 M) was added on to the test paper and left for an hour for adsorption. Followed by this period $NaBH_4$ (10 mM) was added on to the test paper, an immediate visible color change was observed on the filter paper from white to light pink. The test strips were air dried at room temperature. Upon treatment with Cu(II) the pads exhibited a light bluish color compared to the untreated (blank) strips, as illustrated in **Figure 5A**. These visually responsive test strips present a user-friendly, cost-effective, and environmentally sustainable approach for Cu(II) detection. To assess storage stability, the strips were kept at for a duration of one

 doi:10.20944/preprints202508.1109.v1

month, during which they retained their functionality, indicating strong shelf life and reliability for detecting Cu(II). The test strips demonstrated high selectivity toward Cu(II) with a distinct color transition from pink to blue and eventually to dark blue with increasing concentrations of Cu (II) (**Figure 5B**).

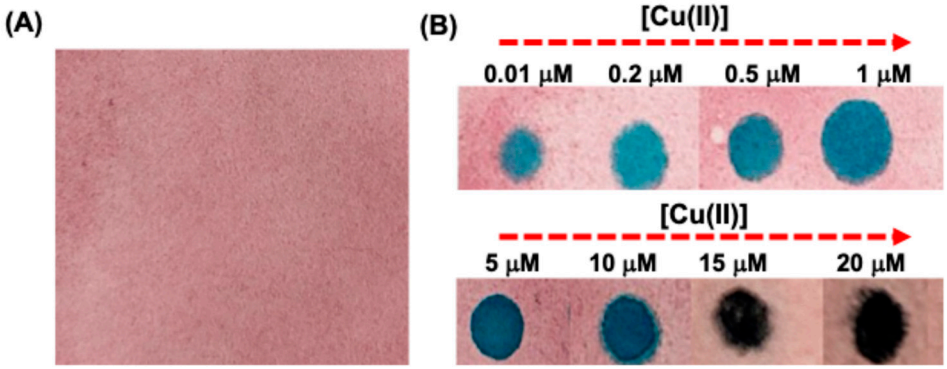

Figure 5. Paper strip-based sensing of Cu(II). (A) Test strip prepared from CW-AuNPs. (B) Colorimetric response of paper strip with varying concentration of Cu(II).

3.4. Surface-Enhanched Raman Spectroscopy Based Detection

Controlled manipulation of nanoparticle aggregation can significantly amplify the formation of localized electromagnetic fields, commonly known as "hot spots," which are highly advantageous for SERS applications. **Figure 6A** illustrates the underlying concept of using SERS nanoprobe technology to detect Cu(II). This detection relies on the unique interaction between **CW** and Cu(II), resulting in alterations in the SERS intensity of **CW** appended to AuNPs. These intensity changes are directly proportional to the concentration of Cu(II). Cu(II) can bind with the free amino groups and the indole moiety of **CW** strongly and resulted in aggregation of **CW**-AuNPs. As shown in **figure 3E**, **CW** powder sample barely showed any vibrational characteristics in the Raman spectrum. But incorporation of **CW** to AuNPs showed vibrational peaks with an enhanced Raman signal intensity for the characteristic functional moieties in **CW**. In this context, when **CW**-AuNPs are exposed to Cu(II) ions, they exhibit an aggregation phenomenon, by leveraging this aggregation behavior, the detection of Cu(II) can be achieved using more sensitive SERS technique. The addition of Cu(II) induces changes in the characteristic Raman peaks of **CW**-AuNPs, and these changes exhibit a linear correlation with the concentration of Cu(II). Raman analysis was performed on both the solution and solid states (Raman mapping) in the presence of Cu(II). The aggregation of **CW**-AuNPs with Cu(II) leads to an enhancement in the Raman intensity, thus improving the SERS signal of the system. Here **CW** act as a Raman reporter and which showed enhanced SERS due to aggregation of AuNPs by Cu (II) to form the so-called hot spots.

As shown in **Figure 6B**, addition of Cu (II) increased the SERS intensity of **CW**-AuNPs. To optimize the sensitivity of copper ion detection, we relied on the SERS peak at at 1416 cm^{-1} because of its high intensity after copper-induced aggregation. According to the strategy of Cu(II) detection, the concentration of Cu(II) plays an essential role in aggregation of **CW**-AuNPs and in the formation of hot-spots for SERS based detection. Thus, Raman spectral changes of **CW**-AuNPs were monitored using varying concentrations of Cu(II) from $1x10^{-5}$ M to $1x10^{-15}$ M. The dose dependent curve showed a linear correlation for the most intense Raman peak in **CW** with varying concentrations of Cu (II) (**Figure 6C**). It was observed that **CW**-AuNPs showed a detectable Raman intensity for the peak even at a lower concentration of Cu(II) such as 10 nM, indicating a highly sensitive detection platform than the optical spectroscopy-based detection. We have studied the selectivity in Cu(II) detection using SERS study using other potential competitive metal ions. Interestingly SERS studies showed a Raman signal enhancement for the peak at 1416 cm-1, for Cu(II) even in the presence of other metal ions tested (**Figure 6D**). Raman mapping studies were performed for **CW**-AuNPs with varying

 doi:10.20944/preprints202508.1109.v1

concentration of Cu(II) (**Figure 6E**). Since Raman mapping is performed with dry samples it offers an enhanced aggregation, and in turn hot-spot formation for SERS applications. The mapping images showed a detectable signal pattern with bright spots for a lower concentration of Cu(II) up to 10 pM (**Figure 6F**). The bright red spots indicate a measure of the Raman spectrum intensity for the peak at 1416 cm^{-1} (**Figure 6F**). Thus, both solution state and dry Raman mapping studies improved the detection limit for Cu (II) using **CW**-AuNPs as compared to optical spectroscopic based detection methods.

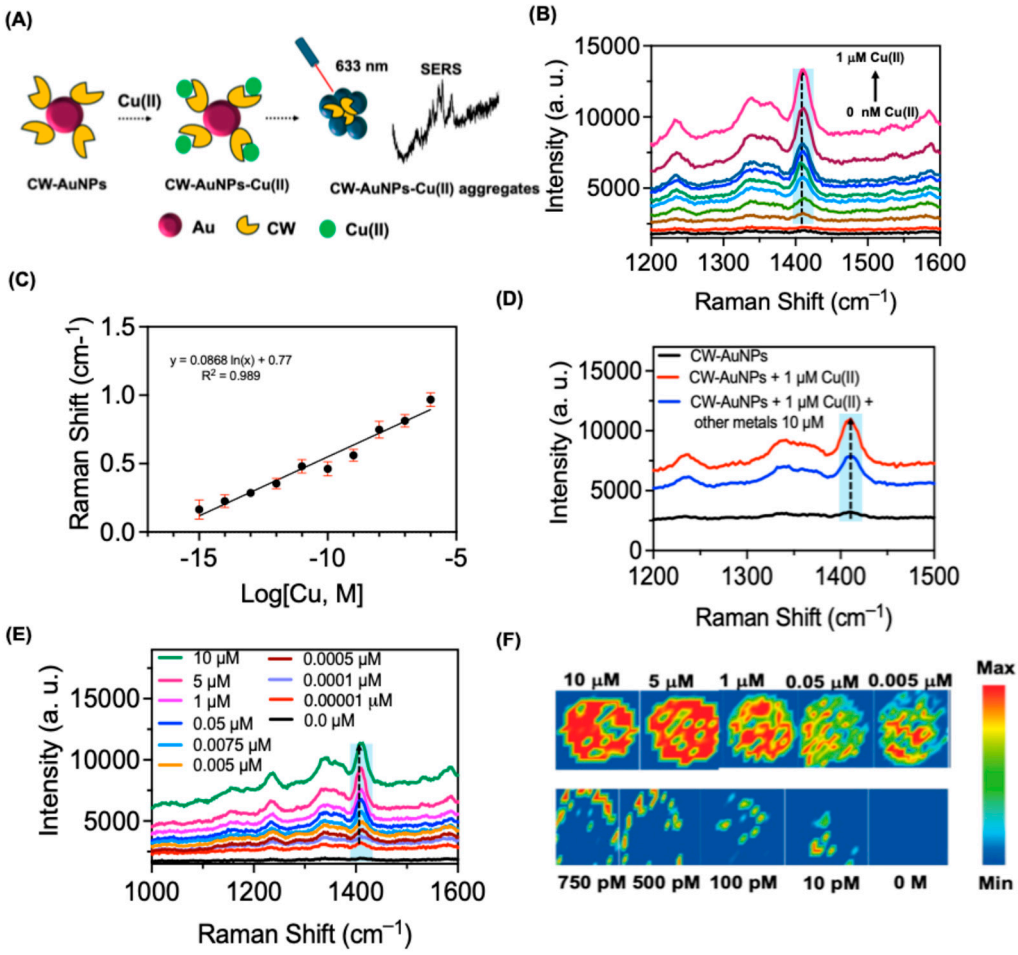

Figure 6. SERS based copper detection. (A) A schematic representation for the SERS based Cu(II) detection using **CW**-AuNPs. (B) Raman spectra for **CW**-AuNPs (50 μg/mL) with the addition of various amounts of Cu(II). (C) Linear relationship between SERS peak intensities at 1416 cm^{-1} and Cu(II) concentrations. (D) Raman spectra for **CW**-AuNPs, **CW**-AuNPs + Cu(II) and **CW**-AuNPs + Cu(II) + various other metal ions. Studies showed high selectivity of **CW**-AuNPs with Cu(II), even with the addition of various other metal ions. (E) SERS for the dried samples of **CW**-AuNPs with Cu(II). Blue shade box indicated Raman Shift at 1416 cm^{-1}. (F) Raman mapping images for the dried samples from **CW**-AuNPs with various concentrations of Cu(II). Excitation: 633 nm laser (6.8 mW); exposure time: 10 s.

4. Activatable Photosensitisation and Biomedical Application

Activatable photosensitizers offer precise spatiotemporal control in photodynamic therapy (PDT) by responding to specific tumor microenvironment cues such as pH, enzymes, and hypoxia, thereby improving selectivity and therapeutic outcomes. We examined the photosensitization behavior of **CW**-AuNPs-Cu nanoaggregates under light irradiation and confirmed their reactive oxygen species (ROS) generation using Singlet Oxygen Sensor Green (SOSG). Among the ROS produced, singlet oxygen plays a key role in enhancing PDT efficacy [45]. SOSG, a selective singlet

 doi:10.20944/preprints202508.1109.v1

oxygen probe, is non-fluorescent under normal conditions but emits at 520 nm upon reaction with singlet oxygen [46]. In our experiments, **CW**-AuNPs-Cu mixed with SOSG and irradiated through a 500 nm band-pass filter displayed a marked fluorescence at 520 nm, confirming singlet oxygen production (**Figure 7A**). No fluorescence was detected in control experiments conducted in the dark or with sodium azide, a singlet oxygen quencher, verifying the photosensitizer's specificity (**Figure 7B**). Using methylene blue as a reference, the singlet oxygen quantum yield (ΦΔ) was determined to be 0.21.

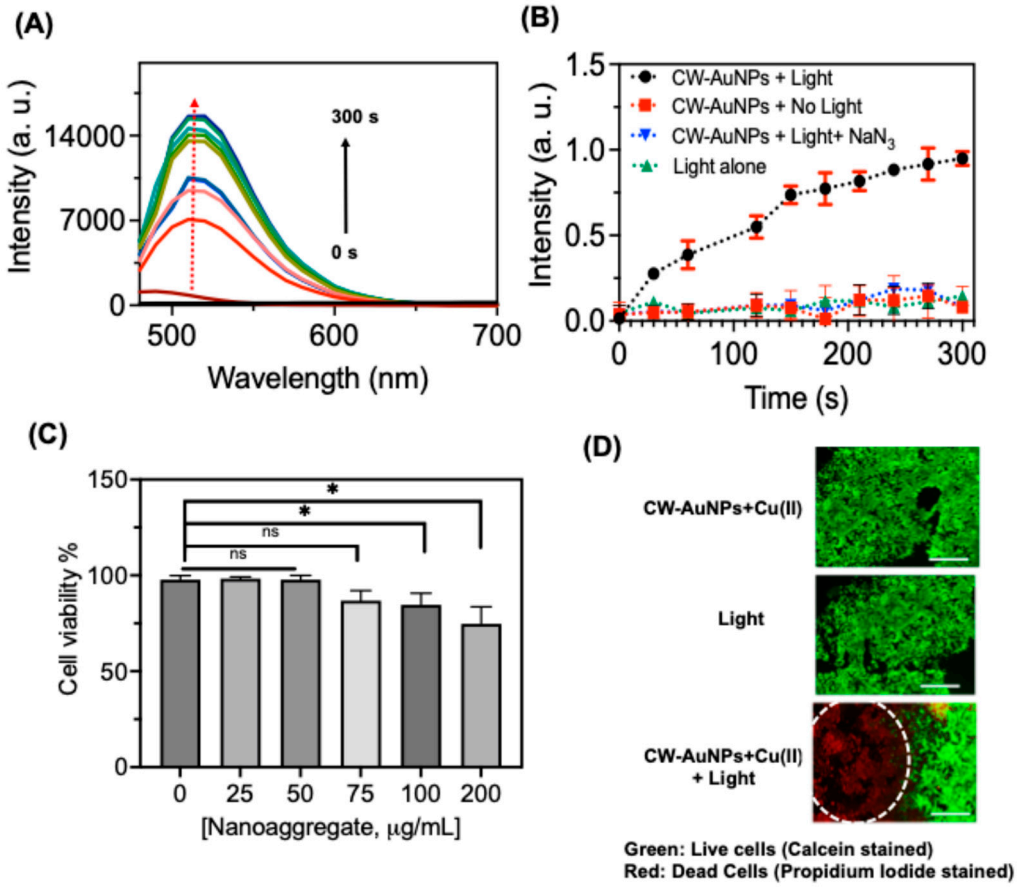

Figure 7. ROS generation from **CW**-AuNPs-Cu nanoaggregate. (A) Time dependant fluorescence spectra (λexc =490 nm; λem =520 nm) of SOSG solutions (5 μM) after exposure with **CW**-AuNPs-Cu nanoaggreate (50 mg/mL) under light. (B) A comparative plot for the fluorescence from SOSG under different conditions. (C) Cell viability assay for **CW**-AuNPs-Cu nanoaggregate on MDMBA cell lines. Where ns- statistically non-significant; *p< 0.05. (D) Live and dead staining studies for MDMBA cells after exposure of 808 nm laser for 2 minutes. The white circles show the area of laser exposure. Scale bar 50 μm. .

For biological validation, the nanoaggregates were evaluated in MDMBA tumor cells. The cytotoxicity of nanoaggregates was tested, and it was shown that for higher concentrations such as 75, 100, and 200 μg/mL, the nanoaggregates showed cytotoxicity (**Figure 7C**). So, we have performed the in vitro experiments at a concentration of 50 mg/μL. Following incubation, cells were exposed to an 808 nm laser at 2 W/cm² for 1 minute. Live/dead staining revealed significant laser-induced cell death (red fluorescence) in treated samples compared to non-irradiated controls, demonstrating the potential of **CW**-AuNPs-Cu nanoaggregates as effective PDT agents (**Figure 7D**).

5. Discussion

The present work introduces a peptide-functionalized gold nanoparticle (**CW**-AuNPs) platform that achieves ultra-sensitive and selective detection of Cu(II) ions through a synergistic combination

 doi:10.20944/preprints202508.1109.v1

of peptide recognition and plasmonic signal amplification. The **CW** peptide, rich in tryptophan and cystine residues, facilitates strong coordination with Cu(II), triggering nanoparticle aggregation and inducing distinct optical changes. This aggregation not only alters the surface plasmon resonance band but detectable by colorimetric and UV-Vis measurements but also generates nanoscale "hot spots" that dramatically enhance Raman scattering signals, enabling detection down to 10 pM in SERS-based assays. Such detection limits surpass most reported peptide nanoparticle sensors, highlighting the exceptional signal enhancement achievable via controlled nanostructure assembly. Importantly, the **CW**-AuNPs retained high specificity in the presence of competing biologically relevant metal ions, which is critical for deployment in complex biological and environmental samples. The development of a solid-phase sensing format, in the form of functionalized paper strips, further underscores the practicality of the platform for rapid, on-site Cu(II) monitoring without the need for sophisticated instrumentation. A comparative analysis with previously reported Cu(II) sensors (Table 1) highlights the superior sensitivity of the CW-AuNPs platform, with detection limits several orders of magnitude lower than most nanoparticle- or peptide-based probes, alongside excellent selectivity.

Table 1. Comparison of reported Cu(II) detection systems with the present **CW**-AuNPs platform.

Sensor type	Mode of detection	Limit of detection	Ref
Julolidine-containing naphthol-based probe	Colorimetric	2 μM	[47]
Gold nanoparticles (AuNPs)	Colorimetric and UV-visible	0.04 μM	[48]
Papain-functionalized AuNPs	Colorimetric	200 nM	[49]
Silver-coated gold nanoparticles	Colorimetric	1 nM	[50]
H-CVNITKQHTVTTTT-NH_2 (Peptide)	Electrochemical	80 nM	[51]
peptide–chelator	Fluorescence	2 μM	[52]
Up conversion lanthanides	Luminescence	37 nmol/L	[53]
Molecularly imprinted nanofilm	Surface plasmon resonance	0.027 μM	[54]
Molecularly imprinted nanoparticles	Surface plasmon resonance	NA	[55]
Pyridine-AuNPs	SERS	50 nM	[34]
Silver nanoparticles	SERS	10pM	[56]
Peptide-AuNPs	SERS, Colorimetric, Fluorescence, Paper strip	0.3 ◉M by optical spectroscopy 76 nM with SPR detection 10 pM by SERS	Present work

Beyond sensing, the **CW**-AuNPs–Cu(II) aggregates exhibited notable photodynamic therapy (PDT) potential, with a singlet oxygen quantum yield of 0.21% and significant phototoxicity against cancer cells upon laser irradiation. The ability to combine ultrasensitive detection with therapeutic functionality positions this system as a promising theranostic nanoplatform, particularly for conditions where copper dysregulation is implicated, such as Wilson's disease or certain malignancies. Future investigations should focus on validating the sensor's performance in real

 doi:10.20944/preprints202508.1109.v1

biological fluids, optimizing PDT efficiency through ligand engineering or nanoparticle morphology control, and assessing in vivo biocompatibility and clearance of the system. Overall, this dual-function **CW**-AuNPs construct bridges the gap between rapid diagnostics and targeted therapy, offering a versatile approach to precision nanomedicine.

6. Conclusion

In summary we have successfully demonstrated a peptide-gold nanoparticle system with multimode detection capability for Cu(II) metal ions. The prepared **CW**-AuNPs, leverage the advantage of peptide moiety for selective and sensitive binding of Cu(II) among all other metal ions tested. The NPs showed colorimetric, optical and SERS based sensitive detection for Cu(II). The optical based detection allowed a sensitivity upto 76 nM, whereas the SERS based study offered 10 pM, with high reproducibility for both solution and mapping studies. A paper strip developed from this NPs, allowed onsite application for the detection of Cu(II). The nanoaggregate from peptide NPs, showed enhanced ROS generation with PDT applications in vitro, with a singlet oxygen quantum yield of 0.21. Overall, our results highlight the potential of peptide-AuNP conjugates as a versatile and robust platform for copper ion detection, addressing current challenges in sensitivity, selectivity, and cost-effectiveness. Future studies could extend this strategy to multiplex sensing or real-sample testing in complex matrices such as serum, wastewater, and food extracts.

Supplementary Materials: The following supporting information can be downloaded at the website of this paper posted on Preprints.org. **Figure S1**: ^{1}H NMR spectrum (D_2O, 300 MHz) of **CW**; **Figure S2**. ^{13}C NMR spectrum (D_2O, 75 MHz) of **CW**; **Figure S3**. Mass spectrometry data for **CW**. **Figure S4**. Photophysics for **CW**; **Figure S5**. Metal ion selectivity study for **CW** with various metal ions; **Table S1**: Time resolved spectroscopic data; **Figure S6**. Binding constant and stoichiometry measurements. **Figure S7**. FT-IR data for **CW**-AuNPs; **Figure S8**. Metal ion selectivity study for **CW-AuNPs** with various metal ions.

Funding: KU-KIST Graduate School of Converging Science and Technology and the BK21 fellowship program, Korea University. Science and Engineering Research Board, New Delhi, India (PDF/2017/001221).

Institutional Review Board Statement: Not applicable.

Informed Consent Statement: Not applicable.

Data Availability Statement: The data can be made available on request.

Acknowledgments: P.K shows sincere gratitude to Dong-Kwon Lim, KUKIST, South Korea and BK21 fellowship program, South Korea. P. K acknowledges Prakash P. Neelakandan, INST, Mohali, Punjab, India, for accepting the short-term visit to his lab and the help provided by him for the synthesis of **CW** peptide. The author acknowledges the instrumentation facilities in KUKIST and INST Mohali for this work.

Conflicts of Interest: Declare no conflicts of interest.

References

1. Moustakas, M. The Role of Metal Ions in Biology, Biochemistry and Medicine. *Materials* **2021**, *14*, 549, doi:10.3390/ma14030549.
2. Turner, R.J. The Good, the Bad, and the Ugly of Metals as Antimicrobials. *Biometals* **2024**, *37*, 545–559, doi:10.1007/s10534-023-00565-y.
3. Attar, T. A Mini-Review on Importance and Role of Trace Elements in the Human Organism. *Chem. Rev. Lett.* **2020**, *3*, doi:10.22034/crl.2020.229025.1058.
4. Gaetke, L.M.; Chow-Johnson, H.S.; Chow, C.K. Copper: Toxicological Relevance and Mechanisms. *Arch. Toxicol.* **2014**, *88*, 1929–1938, doi:10.1007/s00204-014-1355-y.

 doi:10.20944/preprints202508.1109.v1

5. Shabbir, Z.; Sardar, A.; Shabbir, A.; Abbas, G.; Shamshad, S.; Khalid, S.; Natasha; Murtaza, G.; Dumat, C.; Shahid, M. Copper Uptake, Essentiality, Toxicity, Detoxification and Risk Assessment in Soil-Plant Environment. *Chemosphere* **2020**, *259*, 127436, doi:10.1016/j.chemosphere.2020.127436.
6. Hill, S.J.; Fisher, A.S. Atomic Absorption, Methods and Instrumentation. In *Encyclopedia of Spectroscopy and Spectrometry*; Elsevier, 2017; pp. 37–43 ISBN 978-0-12-803224-4.
7. Liu, Y.; Hu, Z.; Gao, S.; Günther, D.; Xu, J.; Gao, C.; Chen, H. In Situ Analysis of Major and Trace Elements of Anhydrous Minerals by LA-ICP-MS without Applying an Internal Standard. *Chemical Geology* **2008**, *257*, 34–43, doi:10.1016/j.chemgeo.2008.08.004.
8. Goullé, J.-P.; Mahieu, L.; Castermant, J.; Neveu, N.; Bonneau, L.; Lainé, G.; Bouige, D.; Lacroix, C. Metal and Metalloid Multi-Elementary ICP-MS Validation in Whole Blood, Plasma, Urine and Hair. *Forensic Sci. Int.* **2005**, *153*, 39–44, doi:10.1016/j.forsciint.2005.04.020.
9. Buffle, J.; Tercier-Waeber, M.-L. Voltammetric Environmental Trace-Metal Analysis and Speciation: From Laboratory to in Situ Measurements. *TrAC, Trends Anal. Chem.* **2005**, *24*, 172–191, doi:10.1016/j.trac.2004.11.013.
10. Lu, M.; Fu, X.; Xie, H.; Liu, M.; Wei, P.; Zhang, W.; Xie, Y.; Qi, Y. Colorimetric Determination of Copper Ion Based on the Silver-Coated Gold Nanobipyramids. *J. Food Compos. Anal.* **2023**, *120*, 105363, doi:10.1016/j.jfca.2023.105363.
11. Cai, R.; Shoukat, C.A.; Zhang, C.; Gao, X.; Li, H.; Chen, J.; Ji, Y.; Wu, X. A Colorimetric Chemosensor for Sensitive and Selective Detection of Copper(Ⅱ) Ions Based on Catalytic Oxidation of 1-Naphthylamine. *Analyst* **2023**, *148*, 3306–3311, doi:10.1039/D3AN00536D.
12. Wang, Y.-R.; Tan, Y.-W.; Zhang, A.-H.; Li, Y.-Y.; Hu, J.-L.; Wu, J.-R.; Tian, Z.-Q.; Ting-Liang; Kang, Y.-F. The Highly Selective and Sensitive Fluorescence Probe for Detection of Copper (II) Ions and Its Bioimaging in Vitro and Vivo. *Spectrochim Acta A Mol. Biomol. Spectrosc.* **2024**, *316*, 124328, doi:10.1016/j.saa.2024.124328.
13. Wang, H.; Cui, J.; Fang, X.; Zhang, W.; Wang, J.; Chen, S.; Qian, J. Fluorescent Detection of Copper Ions with Acylhydrazine-Based Probes: Effects of Substitute and Its Position. *Dyes and Pigments* **2022**, *197*, 109954, doi:10.1016/j.dyepig.2021.109954.
14. Paranawithana, N.N.; Martins, A.F.; Clavijo Jordan, V.; Zhao, P.; Chirayil, S.; Meloni, G.; Sherry, A.D. A Responsive Magnetic Resonance Imaging Contrast Agent for Detection of Excess Copper(II) in the Liver *In Vivo*. *J. Am. Chem. Soc.* **2019**, *141*, 11009–11018, doi:10.1021/jacs.8b13493.
15. Shah, A.; Taylor, M.J.; Molinaro, G.; Anbu, S.; Verdu, M.; Jennings, L.; Mikulska, I.; Diaz-Moreno, S.; El Mkami, H.; Smith, G.M.; et al. Design of the Elusive Proteinaceous Oxygen Donor Copper Site Suggests a Promising Future for Copper for MRI Contrast Agents. *Proc. Natl. Acad. Sci. U.S.A.* **2023**, *120*, e2219036120, doi:10.1073/pnas.2219036120.
16. Sannok, T.; Wechakorn, K.; Jantra, J.; Kaewchoay, N.; Teepoo, S. *Anal. Bioanal. Chem.* **2023**, *415*, 4703–4712, doi:10.1007/s00216-023-04754-z.
17. Amalraj, A.; Ayyanu, R.; Pavadai, R.; Govindaraj, T.S.; Aham, E.C.; Li, X.; Deng, Y.; Zhang, Z. Smartphone Assisted Paper Strip-Based Colorimetric Sensing of Phosphate and Copper Ions Utilizing Bi-Ligand Intercalated Cobalt-MOF as a Dual Functional Nanozyme. *J. Environ. Chem. Eng.* **2024**, *12*, 113522, doi:10.1016/j.jece.2024.113522.
18. Kumalasari, M.R.; Alfanaar, R.; Andreani, A.S. Gold Nanoparticles (AuNPs): A Versatile Material for Biosensor Application. *Talanta Open* **2024**, *9*, 100327, doi:10.1016/j.talo.2024.100327.
19. Ferrari, E. Gold Nanoparticle-Based Plasmonic Biosensors. *Biosensors* **2023**, *13*, 411, doi:10.3390/bios13030411.

 doi:10.20944/preprints202508.1109.v1

20. Kumar, N.; Singh, A.; Dhaka, P.; Singh, A.; Agarwala, P.; Sharma, K.; Bhargava, A.; Bhatia, S.; Launey, T.; Kaushik, R.; et al. A Label-Free Gold Nanoparticles Functionalized Peptide Dendrimer Biosensor for Visual Detection of Breakthrough Infections in COVID-19 Vaccinated Patients. *Sens. Bio-Sens. Res.* **2025**, *47*, 100718, doi:10.1016/j.sbsr.2024.100718.
21. Parnsubsakul, A.; Oaew, S.; Surareungchai, W. Zwitterionic Peptide-Capped Gold Nanoparticles for Colorimetric Detection of Ni^{2+}. *Nanoscale* **2018**, *10*, 5466–5473, doi:10.1039/C7NR07998B.
22. Luo, Y.; Zhang, Y.; Xiong, Z.; Chen, X.; Sha, A.; Xiao, W.; Peng, L.; Zou, L.; Han, J.; Li, Q. Peptides Used for Heavy Metal Remediation: A Promising Approach. *Int. J. Mol. Sci.* **2024**, *25*, 6717, doi:10.3390/ijms25126717.
23. Haridas, V.; Praveen Kumar, P.P.; Suresh, C.H. Cysteine-Based Fluorescence "Turn-on" Sensors for Cu^{2+} and Ag^{+}. *RSC Adv.* **2014**, *4*, 56539–56542, doi:10.1039/C4RA10936H.
24. Boas, D.; Remennik, S.; Reches, M. Peptide-Capped Au and Ag Nanoparticles: Detection of Heavy Metals and Photochemical Core/Shell Formation. *J. Colloid. Interface Sci.* **2023**, *631*, 66–76, doi:10.1016/j.jcis.2022.10.154.
25. Shinde, S.; Kim, D.-Y.; Saratale, R.; Syed, A.; Ameen, F.; Ghodake, G. A Spectral Probe for Detection of Aluminum (III) Ions Using Surface Functionalized Gold Nanoparticles. *Nanomaterials* **2017**, *7*, 287, doi:10.3390/nano7100287.
26. Catanzaro, L.; Scardaci, V.; Scuderi, M.; Condorelli, M.; D'Urso, L.; Compagnini, G. Surface Plasmon Resonance of Gold Nanoparticle Aggregates Induced by Halide Ions. *Mater. Chem. Phys.* **2023**, *308*, 128245, doi:10.1016/j.matchemphys.2023.128245.
27. Tian, F.; Bonnier, F.; Casey, A.; Shanahan, A.E.; Byrne, H.J. Surface Enhanced Raman Scattering with Gold Nanoparticles: Effect of Particle Shape. *Anal. Methods* **2014**, *6*, 9116–9123, doi:10.1039/C4AY02112F.
28. Inoue, Y.; Yoshinare, Y.; Yamaguchi, A.; Oshima, A.; Yamaguchi, M.; Heya, A.; Sumitomo, K. Aggregation Control of Gold Nanoparticles and Surface-Enhanced Raman Scattering within Giant Unilamellar Vesicles. *Langmuir* **2025**, *41*, 9567–9573, doi:10.1021/acs.langmuir.5c00730.
29. Lin, C.; Li, Y.; Peng, Y.; Zhao, S.; Xu, M.; Zhang, L.; Huang, Z.; Shi, J.; Yang, Y. Recent Development of Surface-Enhanced Raman Scattering for Biosensing. *J. Nanobiotechnol.* **2023**, *21*, 149, doi:10.1186/s12951-023-01890-7.
30. Kumar, P.P.P.; Saxena, S.; Joshi, R. Advancements in SERS: Revolutionizing Biomedical Analysis and Applications. *Nanotheranostics* **2025**, *9*, 216–261, doi:10.7150/ntno.106396.
31. Kumar, P.P.P.; Suresh, C.H.; Haridas, V. A Supramolecular Approach to Metal Ion Sensing: Cystine-Based Designer Systems for Cu^{2+} , Hg^{2+} , Cd^{2+} and Pb^{2+} Sensing. *RSC Adv.* **2015**, *5*, 7842–7847, doi:10.1039/C4RA14389B.
32. Yin, J.; Wu, T.; Song, J.; Zhang, Q.; Liu, S.; Xu, R.; Duan, H. SERS-Active Nanoparticles for Sensitive and Selective Detection of Cadmium Ion (Cd^{2+}). *Chem. Mater.* **2011**, *23*, 4756–4764, doi:10.1021/cm201791r.
33. Song, C.; Yang, B.; Zhu, Y.; Yang, Y.; Wang, L. Ultrasensitive Sliver Nanorods Array SERS Sensor for Mercury Ions. *Biosens Bioelectron.* **2017**, *87*, 59–65, doi:10.1016/j.bios.2016.07.097.
34. Dugandžić, V.; Kupfer, S.; Jahn, M.; Henkel, T.; Weber, K.; Cialla-May, D.; Popp, J. A SERS-Based Molecular Sensor for Selective Detection and Quantification of Copper(II) Ions. *Sensors and Actuators B: Chemical* **2019**, *279*, 230–237, doi:10.1016/j.snb.2018.09.098.
35. Sapra, R.; Gupta, M.; Khare, K.; Chowdhury, P.K.; Haridas, V. Fluorescence by Self-Assembly: Autofluorescent Peptide Vesicles and Fibers. *Analyst* **2023**, *148*, 973–984, doi:10.1039/D3AN00124E.
36. Shao, J.; Kuiper, B.P.; Thunnissen, A.-M.W.H.; Cool, R.H.; Zhou, L.; Huang, C.; Dijkstra, B.W.; Broos, J. The Role of Tryptophan in π Interactions in Proteins: An Experimental Approach. *J. Am. Chem. Soc.* **2022**, *144*, 13815–13822, doi:10.1021/jacs.2c04986.

 doi:10.20944/preprints202508.1109.v1

37. Yugay, D.; Goronzy, D.P.; Kawakami, L.M.; Claridge, S.A.; Song, T.-B.; Yan, Z.; Xie, Y.-H.; Gilles, J.; Yang, Y.; Weiss, P.S. Copper Ion Binding Site in β-Amyloid Peptide. *Nano Lett.* **2016**, *16*, 6282–6289, doi:10.1021/acs.nanolett.6b02590.
38. Wärmländer, S.; Tiiman, A.; Abelein, A.; Luo, J.; Jarvet, J.; Söderberg, K.L.; Danielsson, J.; Gräslund, A. Biophysical Studies of the Amyloid β-Peptide: Interactions with Metal Ions and Small Molecules. *Chem.Bio.Chem.* **2013**, *14*, 1692–1704, doi:10.1002/cbic.201300262.
39. Brynn Hibbert, D.; Thordarson, P. The Death of the Job Plot, Transparency, Open Science and Online Tools, Uncertainty Estimation Methods and Other Developments in Supramolecular Chemistry Data Analysis. *Chem. Commun.* **2016**, *52*, 12792–12805, doi:10.1039/C6CC03888C.
40. Thordarson, P. Determining Association Constants from Titration Experiments in Supramolecular Chemistry. *Chem. Soc. Rev.* **2011**, *40*, 1305–1323, doi:10.1039/C0CS00062K.
41. Chatterjee, S.; Lou, X.-Y.; Liang, F.; Yang, Y.-W. Surface-Functionalized Gold and Silver Nanoparticles for Colorimetric and Fluorescent Sensing of Metal Ions and Biomolecules. *Coord. Chem. Rev.* **2022**, *459*, 214461, doi:10.1016/j.ccr.2022.214461.
42. Praveen Kumar, P.P.; Kathuria, L.; Haridas, V. Cysteine-Based Silver Nanoparticles as Dual Colorimetric Sensors for Cations and Anions. *New J. Chem.* **2016**, *40*, 8382–8389, doi:10.1039/C6NJ01486K.
43. Gruszczyńska, E.; Lewkowicz, A.; Czarnomska, M.; Koczur, J.; Walczewska-Szewc, K.; Kaliszan, M.; Balwicki, Ł.; Bojarski, P. Spectroscopic Analysis of Tryptophan as a Potential Optical Biomarker for Estimating the Time of Death. *Int. J. Mo.l Sci.* **2024**, *25*, 12915, doi:10.3390/ijms252312915.
44. Hirakawa, A.Y.; Nishimura, Y.; Matsumoto, T.; Nakanishi, M.; Tsuboi, M. Characterization of a Few Raman Lines of Tryptophan. *J. Raman Spectroscopy* **1978**, *7*, 282–287, doi:10.1002/jrs.1250070511.
45. Maharjan, P.S.; Bhattarai, H.K. Singlet Oxygen, Photodynamic Therapy, and Mechanisms of Cancer Cell Death. *Journal of Oncology* **2022**, *2022*, 1–20, doi:10.1155/2022/7211485.
46. Kim, S.; Fujitsuka, M.; Majima, T. Photochemistry of Singlet Oxygen Sensor Green. *J. Phys. Chem. B* **2013**, *117*, 13985–13992, doi:10.1021/jp406638g.
47. Park, G.J.; Hwang, I.H.; Song, E.J.; Kim, H.; Kim, C. A Colorimetric and Fluorescent Sensor for Sequential Detection of Copper Ion and Cyanide. *Tetrahedron* **2014**, *70*, 2822–2828, doi:10.1016/j.tet.2014.02.055.
48. Deng, H.-H.; Li, G.-W.; Liu, A.-L.; Chen, W.; Lin, X.-H.; Xia, X.-H. Thermally Treated Bare Gold Nanoparticles for Colorimetric Sensing of Copper Ions. *Microchim. Acta* **2014**, *181*, 911–916, doi:10.1007/s00604-014-1184-y.
49. Guo, Y.; Wang, Z.; Qu, W.; Shao, H.; Jiang, X. Colorimetric Detection of Mercury, Lead and Copper Ions Simultaneously Using Protein-Functionalized Gold Nanoparticles. *Biosensors and Bioelectronics* **2011**, *26*, 4064–4069, doi:10.1016/j.bios.2011.03.033.
50. Lou, T.; Chen, L.; Chen, Z.; Wang, Y.; Chen, L.; Li, J. Colorimetric Detection of Trace Copper Ions Based on Catalytic Leaching of Silver-Coated Gold Nanoparticles. *ACS Appl. Mater. Interfaces* **2011**, *3*, 4215–4220, doi:10.1021/am2008486.
51. Magarelli, G.; Da Silva, J.G.; Ribeiro, C.L.; De Freitas, T.V.; Rodrigues, M.A.; De Souza Gil, E.; Marraccini, P.; De Souza, J.R.; De Castro, C.S.P.; Bemquerer, M.P. A Voltammetric Peptide Biosensor for Cu2+ Metal Ion Quantification in Coffee Seeds. *J. Inorg. Biochem.* **2024**, *251*, 112441, doi:10.1016/j.jinorgbio.2023.112441.
52. Nguyen, N.K.; Poduska, B.; Franks, M.; Bera, M.; MacCormack, I.; Lin, G.; Petroff, A.P.; Das, S.; Nag, A. A Copper-Selective Sensor and Its Inhibition of Copper-Amyloid Beta Aggregation. *Biosensors* **2024**, *14*, 247, doi:10.3390/bios14050247.

 doi:10.20944/preprints202508.1109.v1

53. Shi, Y.; Liu, Q.; Yuan, W.; Xue, M.; Feng, W.; Li, F. Dye-Assembled Upconversion Nanocomposite for Luminescence Ratiometric in Vivo Bioimaging of Copper Ions. *ACS Appl. Mater. Interfaces* **2019**, *11*, 430–436, doi:10.1021/acsami.8b19961.
54. Gerdan, Z.; Saylan, Y.; Denizli, A. Recent Advances of Optical Sensors for Copper Ion Detection. *Micromachines* **2022**, *13*, 1298, doi:10.3390/mi13081298.
55. Safran, V.; Göktürk, I.; Derazshamshir, A.; Yılmaz, F.; Sağlam, N.; Denizli, A. Rapid Sensing of Cu+2 in Water and Biological Samples by Sensitive Molecularly Imprinted Based Plasmonic Biosensor. *Microchem. J.* **2019**, *148*, 141–150, doi:10.1016/j.microc.2019.04.069.
56. Liu, Y.; Wu, Y.; Guo, X.; Wen, Y.; Yang, H. Rapid and Selective Detection of Trace Cu2+ by Accumulation-Reaction-Based Raman Spectroscopy. *Sens. Actuators B-Chem.* **2019**, *283*, 278–283, doi:10.1016/j.snb.2018.12.043.